

Remote Binding Energy in Antibody Catalysis: Studies of a Catalytically Unoptimized Specificity Pocket

Herschel Wade and Thomas S. Scanlan*

Contribution from The Departments of Pharmaceutical Chemistry and Cellular and Molecular Pharmacology, University of California, San Francisco, California 94143-0446

Received August 21, 1998

Abstract: Binding interactions remote from the hydrolytic reaction center have been probed with substrate and phosphonate transition state analogues to understand how these types of interactions are used to promote catalysis in the 17E8 system. We find that the hapten-generated recognition pocket in 17E8 has properties that are analogous to those of specificity pockets in enzymes. We have also found that there are specific requirements to form catalytically productive interactions between the side chain and the recognition pocket including conformation, size, and geometry. An additional requirement includes favorable simultaneous interactions between the side chain and binding pocket along with favorable interactions with the oxyanion hole. The 17E8 side chain recognition pocket seems to be less catalytically efficient than analogous pockets in enzymatic systems. The apparent binding energy gained from the methylene–pocket interactions in the 17E8 system is significantly smaller than those observed in natural enzymes. Furthermore, 17E8 does not use specific interactions in the recognition pocket to significantly affect catalytic turnover (k_{cat}) which is thought to be a trait of an unoptimized catalyst. Analysis of the crystal structure of the 17E8·hapten complex has allowed for the identification of differences between the active sites of 17E8 and several proteases. The identified differences give insight to the sources of the inefficient use of binding energy.

Introduction

The use of binding energy to achieve rate accelerations is one feature that distinguishes enzymes from simple catalysts. This notion of translating binding energy into catalysis has been exploited in the generation of enzyme mimics such as catalytic antibodies. These immunoglobulins have been generated against haptens that are designed to create binding sites that use binding energy to promote catalysis.^{1–3} So far, most of the catalytic antibody design efforts have focused on the protein environment proximal to the portion of the substrate that undergoes bond changes. Although there is no doubt that this part of the active site is an essential feature of a catalyst, nature has shown that interactions that occur away from the site of bond cleavage can be used to promote catalysis.^{4–6}

Previous studies suggest that binding interactions away from the catalytic center are essential for catalysis by the antibody 17E8.⁷ This antibody was generated against a phosphonate monoanion and catalyzes the efficient, enantioselective hydrolysis of the phenyl ester of *n*-formylnorleucine.⁸ The crystal structure of the 17E8·hapten complex indicates that there are

several binding interactions that are responsible for 17E8's catalytic properties, including a well-defined pocket for the *n*-butyl side chain of the transition state analogue, and presumably the transition state of the hydrolytic reaction (Figure 1).⁹ Removal of these side chain interactions results in a loss of catalysis, suggesting a role for the 17E8 recognition pocket that is similar to the role of specificity pockets used by natural enzymes, especially those that utilize peptides or amino acids as substrates.^{4,6,10–12}

To study this hapten-generated recognition pocket and the catalytic use of remote binding interactions in the 17E8 mechanism, a series of α -(formylamino)phenyl esters, all of which contain different side chains (Figure 2), were synthesized and used in the 17E8-catalyzed reaction (Scheme 1). In addition, a series of corresponding α -(formylamino)phosphonates were synthesized to probe binding interactions that would occur upon the formation of the hydrolytic transition state or a nearby tetrahedral intermediate (Figure 3). The results from these experiments provide a conceptual framework for how these remote interactions are used in the 17E8 mechanism and how important these interactions are to 17E8 catalysis.¹³

Experimental Section

Synthesis. General Methods and Reagents. Reactions requiring anhydrous conditions were carried out in flame-dried glassware under

* To whom correspondence should be addressed.

(1) Wade, H.; Scanlan, T. S. *Annu. Rev. Biophys. Biomol. Struct.* **1997**, *26*, 461–493.

(2) Shokat, K. M.; Schultz, P. G. *Annu. Rev. Immunol.* **1990**, *8*, 335–363.

(3) Benkovic, S. J. *Annu. Rev. Biochem.* **1992**, *61*, 29–54.

(4) Jencks, W. P. *Catalysis in Chemistry and Enzymology*; Dover Publications: Mineola, 1969.

(5) Jencks, W. P. *Cold Spring Harbor Symp. Quant. Biol.* **1987**, *LII*, 65–73.

(6) Fersht, A. *Enzyme Structure and Mechanism*, 2nd ed.; W. H. Freeman & Co.: New York, 1985; pp 147–149.

(7) Wade, H.; Scanlan, T. S. *J. Am. Chem. Soc.* **1996**, *118*, 6510–6511.

(8) Guo, J.; Huang, W.; Scanlan, T. S. *J. Am. Chem. Soc.* **1994**, *116*, 6062–6069.

(9) Zhou, G. W.; Guo, J.; Huang, W.; Fletterick, R. J.; Scanlan, T. S. *Science* **1994**, *265*, 1059–1064.

(10) Fersht, A. R. *Proc. R. Soc. London B* **1974**, *187*, 397–407.

(11) Fersht, A. R.; Dingwall, C. *Biochemistry* **1979**, *18*, 1245–1249.

(12) Page, M. I. *Angew. Chem., Int. Ed. Engl.* **1977**, *16*, 449–459.

(13) For an example of the design and functional characterization of an antibody binding site that was designed to exhibit broad specificity at the α -substituent of the amino acid substrate see: Tanaka, F., Kinoshita, K., Tanimura, R., Fujii, I. *J. Am. Chem. Soc.* **1996**, *118*, 2332–2339. The relaxation of substrate specificity at this position was accomplished by substituting the α -substituent with the linker.

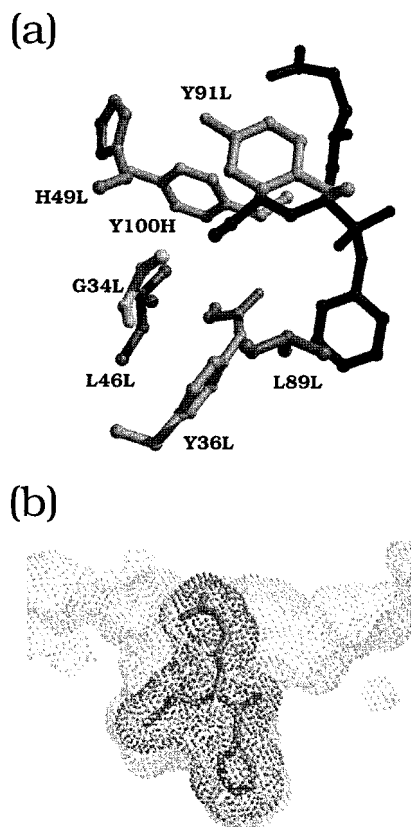


Figure 1. (a) Active site residues proximal to the *n*-butyl side chain of **5p**. The hapten is colored black. The nomenclature for residues consists of (from left to right) the one letter amino acid code, residue number, and designation for the light (L) or heavy (H) chain of the antibody. The figure was generated with the MIDAS program.⁷⁵ (b) Solvent accessible surface of the 17E8 hapten binding site (light gray) complexed with **5p** (black). The surface was generated with a 1.4 Å probe using the MIDAS program.⁷⁶ The coordinates of the complex were taken from the PDB file leap.

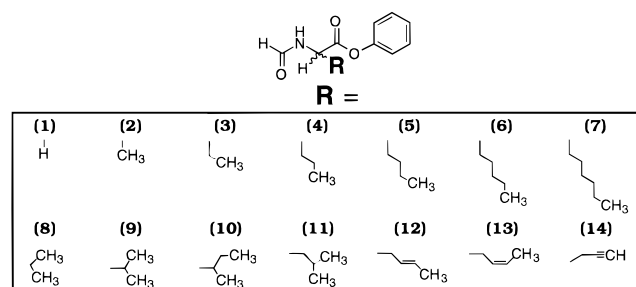


Figure 2. Phenyl esters used to probe the catalytic transition state binding interactions in the 17E8 mechanism. (Top) Substrate skeleton where R represents the position at which the side chain (bottom) was varied. Substrates with side chains correspond to (1–7) the homologous series, (8–11) the branched series, and (12–14) the conformationally restricted series.

an atmosphere of argon. Anhydrous solvents were purchased from Aldrich. Chromatography solvents were purchased from Fisher Corp. and were used as received. Reagents were purchased from either Sigma or Aldrich and used as received unless noted otherwise. ¹H NMR and ¹³C NMR were recorded on a General Electric 300-MHz instrument. The NMR samples were prepared in 5-mm tubes, and the chemical shifts are reported in parts per million (δ) relative to the standards TMS for samples in CDCl₃ and TSP (3-(trimethylsilyl)-1-propanesulfonic acid sodium salt) for samples in D₂O. Flash chromatography was performed with Merck silica gel 60 (230–400 mesh). Ion exchange chromatography was performed with diethylaminoethyl (DEAE) Sephadex A-25 (anion exchange) and Dowex 50WX2-100 (cation exchange).

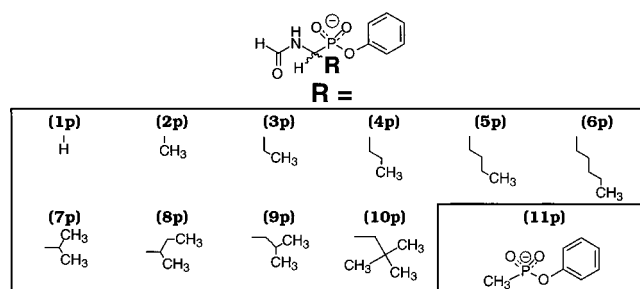
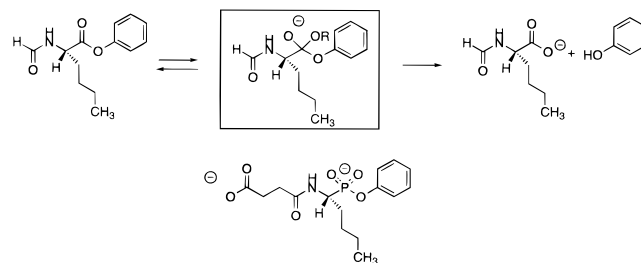


Figure 3. Phosphonate phenyl esters. (Top) Phosphonate skeleton. (Bottom) Side chains. Side chains correspond to (1p–6p, 11p) the homologous series and (7p–10p) the branched series.

Scheme 1. Esterolytic Reaction Catalyzed by 17E8 [(Boxed) Putative High-Energy Tetrahedral Intermediate] and Phosphonate Anion Used To Generate 17E8



The resins were washed and prepared according to manufacturers' recommendations.

Synthesis of *n*-Formylated Amino Acid Ester Substrates, 1–14.

Formylation of Substrates. The amino acids were formylated in the manner as described by Sheehan and Yang.¹⁴ A general procedure for the preparation of the formylated amino acids is as follows: Acetic anhydride (33 mL, 325 mmol) was added dropwise to a solution of *d,l*-norleucine (1.3 g, 10 mmol) dissolved in 100 mL of formic acid. After the addition of acetic anhydride, the solution was stirred at room temperature for 3 h. The mixture was then concentrated by rotary evaporation to yield a white powder. This crude material was carried on directly to the esterification step.

Preparation of Phenyl Esters. The phenyl esters were prepared from the formylated amino acids as described by Castro et al.¹⁵ A general procedure for the esterification of the formylated amino acids is as follows: racemic *n*-formylnorleucine (1 g, 6 mmol), phenol (0.6 g, 6 mmol), triethylamine (1.2 g, 12 mmol), and HBTU (2-(1*H*-benzotriazole-1-yl)-1,1,3,3-tetramethyluronium hexafluorophosphate) (2.3 g, 6 mmol) were dissolved in 50 mL of dichloromethane. The mixture was stirred at room temperature for 3 h. Saturated aqueous NaCl (50 mL) was added to the solution. The solution was then extracted with ethyl acetate (3 × 30 mL). The organic phase was then washed with 2 N HCl (3 × 30 mL), saturated NaHCO₃ (3 × 30 mL), and saturated NaCl (2 × 50 mL). The organic phase was then dried with NaSO₄ and the solvent removed by rotary evaporation to yield a yellow oil, which was chromatographed. Elution of a gradient of (1:5 to 1:1) ethyl acetate–hexanes afforded **5** (1.2 g, 86% yield) as a colorless oil.

***n*-Formylglycine Phenyl Ester (1).** ¹H NMR (300 MHz, CDCl₃) δ 8.32 (s, 1H), 7.42 (t, *J* = 7.5 Hz, 2H), 7.25 (t, *J* = 7.8 Hz, 2H), 7.12 (d, *J* = 7.8 Hz, 1H), 6.29 (br s, 1H), 4.39 (d, *J* = 5.4 Hz, 2H); ¹³C NMR δ 161.2, 129.6, 126.4, 121.2, 40.1; MS (EI) 180.1 (MH⁺), 94.0, 86.0, 65.0, 58.0; HRMS calcd for C₉H₁₀N₁O₃ 180.0661, found 180.0662.

***n*-Formylalanine Phenyl Ester (2).** Yield 0.73 g (88%); ¹H NMR (300 MHz, CDCl₃) δ 8.23 (s, 1H), 7.40 (t, *J* = 7.8 Hz, 2H), 2.23 (t, *J* = 7.5, 7.2 Hz, 1H), 7.10 (d, *J* = 8.1 Hz, 2H), 6.35 (br s, 1H), 4.93 (p, *J* = 7.2 Hz, 1H), 1.62 (d, *J* = 7.2 Hz, 3H); ¹³C NMR δ 160.5, 129.5, 126.3, 121.2, 47.0, 18.4; MS (EI) 194.1 (MH⁺), 165.1, 116.1, 100.0,

(14) Sheehan, J. C.; Yang, D.-D. H. *J. Am. Chem. Soc.* **1958**, *80*, 1154–58.

(15) Castro, B.; Evin, G.; Claude, S.; Seyer, R. *Synthesis* **1977**, 413.

94.0, 82.9, 72.0, 65.0, 55.0; HRMS calcd for $C_{10}H_{21}N_1O_3$ 193.0739, found 193.0748.

***n*-Formyl- α -aminobutyric Phenyl Ester (3).** Yield 0.64 g (80%); 1H NMR (300 MHz, $CDCl_3$) δ 8.28 (s, 1H), 7.40 (t, $J = 7.8$ Hz, 2H), 7.26 (t, $J = 7.5$, 6.9 Hz, 1H), 7.10 (d, $J = 8.1$ Hz, 2H), 6.29 (br s, 1H), 4.93 (q, $J = 6.9$ Hz), 2.19–2.05 (m, 1H), 1.97 (h, $J = 7.2$ Hz, 1H), 1.06 (t, $J = 7.5$ Hz); ^{13}C NMR δ 160.7, 129.6, 126.3, 121.2, 52.0, 25.7, 9.40; MS (EI) 207.1 (M^+), 207.1, 179.1, 133.0, 114.1, 94.0, 86.1, 65.0, 58.1; HRMS calcd for $C_{11}H_{14}N_1O_3$ (MH^+) 208.0974, found 208.0970.

***n*-Formylnorvaline Phenyl Ester (4).** Yield 0.69 g (90%); 1H NMR (300 MHz, $CDCl_3$) δ 8.26 (s, 1H), 7.39 (t, $J = 7.5$ Hz, 2H), 7.26 (t, $J = 7.5$, 7.2 Hz, 1H), 7.06 (d, $J = 8.1$ Hz), 6.30 (br d, $J = 6.0$ Hz, 1H), 4.95 (dt, $J = 7.5$, 5.7 Hz, 1H), 2.09–1.97 (m, 1H), 1.87 (p, $J = 6.9$ –7.5 Hz, 1H), 1.50 (sept, $J = 7.2$, 7.5 Hz, 2H), 1.01 (t, 7.2 Hz, 3H); ^{13}C NMR δ 160.7, 129.5, 126.3, 121.2, 50.8, 34.5, 18.5, 13.6; MS (EI) 222.1 (MH^+), 128.1, 100.1, 94.0, 82.9, 65.0, 58.0; HRMS calcd for $C_{12}H_{16}N_1O_3$ 222.1130 (MH^+), found 222.1133.

***n*-Formylnorleucine Phenyl Ester (5).** Yield 1.2 g (86%); 1H NMR (300 MHz, $CDCl_3$) δ 8.27 (s, 1H), 7.40 (t, $J = 7.8$ Hz, 2H), 7.26 (t, $J = 7.2$, 7.5 Hz, 1H), 7.09 (d, $J = 7.8$ Hz, 2H), 6.21 (br d, $J = 6.0$ Hz, 1H), 4.95 (dt, $J = 7.5$, 5.7 Hz, 1H), 2.16–2.00 (m, 1H), 1.90 (m, 1H), 1.42 (m, 4H), 0.94 (t, $J = 6.9$, 6.6 Hz, 3H); ^{13}C NMR δ 160.7, 129.6, 126.3, 121.2, 51.0, 32.2, 27.2, 22.3, 13.8; MS (EI) 236.1 (MH^+), 207.1, 142.1, 114.1, 94.0, 82.9, 69.1, 58.0; HRMS calcd for $C_{13}H_{18}N_1O_3$ 236.1287 (MH^+), found 236.1296.

***n*-Formyl- α -aminoheptanoic Acid Phenyl Ester (6).** The α -aminoheptanoic acid was synthesized by the method as described by O'Donnell et al using bromopentane.¹⁶ Yield 0.22 g (88%); 1H NMR (300 MHz, $CDCl_3$) δ 8.27 (s, 1H), 7.40 (t, $J = 7.5$ Hz, 2H), 7.26 (t, $J = 7.5$, 7.2 Hz, 1H), 7.09 (d, $J = 8.1$, 2H), 6.19 (d, $J = 7.2$ Hz, 1H), 4.95 (dt, $J = 7.5$, 5.4 Hz, 1H), 2.05 (m, 1H), 1.88 (m, 1H), 1.49, 1.30 (m, 8H), 0.89 (t, $J = 6.6$ Hz, 3H); ^{13}C NMR δ 160.5, 129.5, 126.3, 121.2, 51.0, 32.5, 31.3, 24.8, 22.4, 13.9; MS (EI) 250.1 (MH^+), 156.1, 128.1, 94.0, 83.1, 58.0; HRMS calcd for $C_{14}H_{20}N_1O_3$ (MH^+) 250.1443, found 250.1440.

***n*-Formyl- α -aminohexanoic Acid Phenyl Ester (7).** Yield 0.62 g (88%); 1H NMR (300 MHz, $CDCl_3$) δ 8.33 (s, 1H), 7.42 (t, $J = 7.5$ Hz, 2H), 7.26 (t, $J = 7.2$ Hz, 1H), 7.10 (d, 7.8 Hz, 2H), 6.19 (br d, $J = 6.3$ Hz, 1H), 4.9 (dt, $J = 6.9$, 6.3 Hz, 1H), 2.05 (m, Hz, 1H), 1.87 (m, 1H), 1.41, 1.31 (m, 8H), 0.90 (t, $J = 5.7$ Hz, 3H); ^{13}C NMR δ MS(EI) 264.2 (MH^+), 235.2, 170.1, 142.1, 114.1, 94.0, 77.0; HRMS calcd for $C_{13}H_{22}NO_3$ (MH^+) 264.1600, found 264.1598

***n*-Formyl- α -aminoisobutyric Acid Phenyl Ester (8).** Yield 0.47 g (60%); 1H NMR (300 MHz, $CDCl_3$) δ 8.16 (s, 1H), 7.39 (t, $J = 7.5$, 7.8, 2H), 7.24 (t, $J = 6.9$, 7.2, 1H), 7.10 (d, $J = 7.8$, 2H), 6.25 (br s, 1H), 1.75 (s, 6H); ^{13}C NMR δ 160.5, 129.5, 126.0, 121.3, 56.2, 24.8; MS (EI) 208.1 (MH^+) 179.1, 147.0, 114.1, 94.0, 86.1, 65.0, 58.1; HRMS calcd for $C_{11}H_{13}NO_3$ (MH^+) 208.0974, found 208.0983.

***n*-Formylvaline Phenyl Ester (9).** Yield 0.58 g (75%); 1H NMR (300 MHz, $CDCl_3$) δ 8.38 (s, 1H), 7.46 (t, $J = 7.5$, 7.8 Hz, 2H), 7.32 (t, $J = 6.6$ Hz, 1H), 7.15 (d, 7.8 Hz, 2H), 6.21 (br d, $J = 6.0$ Hz, 1H), 4.99 (dd, $J = 9.0$, 4.5 Hz, 1H), 2.46 (h, $J = 6.9$ Hz, 1H), 1.15, 1.12 (d, $J = 6.9$ Hz, d, $J = 7.2$ Hz 6H); ^{13}C NMR δ 170.3, 160.9, 150.3, 129.6, 126.3, 121.3, 55.7, 31.4, 19.0, 17.7; MS (EI) 222.2 (MH^+), 128.1, 100.1, 94.0, 85.0, 72.1, 65.0; HRMS calcd for (MH^+) 222.1130, found 222.1135.

***n*-Formylleucine Phenyl Ester (10).** Yield 0.66 g (89%); 1H NMR (300 MHz, $CDCl_3$) δ 8.24 (s, 1H), 7.39 (t, $J = 7.5$, 7.8 Hz, 2H), 7.25 (t, $J = 7.2$ Hz, 1H), 7.10 (d, $J = 8.1$ Hz, 2H), 6.30 (br d, 7.5 Hz, 1H), 4.99–4.92 (m, 1H), 1.90–1.67 (m, 3H), 1.02 (d, $J = 5.7$, 6H); ^{13}C NMR δ 171.3, 160.8, 129.5, 126.2, 121.2, 49.5, 41.5, 24.9, 22.8, 21.9; MS (EI) 236.1 (MH^+), 207.1, 149.0, 142.1, 133.0, 114.1, 94.0, 86.1, 77.0, 69.1; HRMS calcd for (MH^+) 236.1290, found 236.1295.

***n*-Formylisoleucine Phenyl Ester (11).** Yield 0.52 g (75%); 1H NMR (300 MHz, $CDCl_3$) δ 8.32, 8.30 (s, s 1H), 7.40 (t, $J = 7.5$, 7.8 Hz, 2H), 7.26 (t, $J = 7.2$, 7.5 Hz, 1H), 7.09 (d, $J = 8.1$ Hz, 2H), 6.21, 6.15 (br d, br d, $J = 6.9$ Hz, 1H), 5.07, 4.96 (dd, dd, $J = 9.0$, 3.6 Hz, $J = 8.7$, 4.5 Hz, 1H), 2.17 (m, 1H), 1.57 (m, 1H), 1.34 (m, 1H), 1.06,

1.00 (m, 6H); ^{13}C NMR δ 160.9, 160.7, 129.6, 126.3, 121.2, 55.1, 53.9, 38.2, 37.8, 15.6, 14.6, 11.6, 11.7; MS (EI) 236.1 (MH^+), 142.1, 114.1, 94.0, 82.9, 69.1, 58.0; HRMS calcd for (MH^+) 236.1287, found 236.1290.

***n*-Formyl-*trans*-crotylglycine Phenyl Ester (12).** Yield 0.66 g (89%). 1H NMR (300 MHz, $CDCl_3$) δ 8.26 (s, 1H), 7.39 (t, $J = 7.5$, 7.8 Hz, 2H), 7.28 (t, $J = 6.9$, 7.8 Hz, 1H), 7.08 (d, $J = 7.8$ Hz, 2H), 6.17 (br s, 1H), 5.67 (d qt, $J = 15.0$, 6.3 Hz, 1H), 5.42 (dt, $J = 15.0$, 6.9 Hz, 1H), 4.96 (dt, $J = 7.8$, 5.7 Hz, 1H), 2.71 (t, $J = 6.3$ Hz, 2H), 1.72 (d, $J = 6.3$ Hz, 3H); ^{13}C NMR δ 160.4, 130.9, 126.3, 123.8, 121.2, 50.8, 35.3, 18.0; MS (EI) 233.1 (M^+) 140.1, 112.1, 94.0, 82.9, 67.1; HRMS calcd for $C_{13}H_{15}N_1O_3$ (M^+) 233.1049, found 233.1052.

***n*-Formyl-*cis*-crotylglycine Phenyl Ester (13).** The α -amino-*cis*-4-hexenoic acid was synthesized by the method as described by O'Donnell et al. using *cis*-crotyl bromide.¹⁶ Yield 0.32 g (85%); 1H NMR (300 MHz, $CDCl_3$) δ 8.25 (s, 1H), 7.41 (t, $J = 7.5$, 7.8 Hz, 2H), 7.32 (t, $J = 7.5$ Hz, 1H), 7.20 (d, $J = 7.8$ Hz, 2H), 6.17 (br s, 1H), 5.70 (m, 1H), 5.43 (q, $J = 7.5$ Hz, 1H), 4.97 (m, 1H), 2.80 (m, 1H), 2.70 (t, $J = 6.6$ Hz, 1H), 1.70 (d, $J = 7.2$ Hz, 1H); ^{13}C NMR δ 160.6, 129.5, 129.1, 126.2, 122.8, 121.2, 50.6, 29.5, 13.0; MS (EI) 234.1 (MH^+) 188.1, 154.1, 140.1, 112.1, 94.0, 84.1, 77.0, 67.1; HRMS calcd for $C_{13}H_{15}NO_3$ (M^+) 234.1130, found 234.1129.

1-Amino-*cis*-4-hexenoic Acid. 1H NMR (300 MHz, $CDCl_3$) δ 5.80 (m, 1H), 5.40 (m, 1H), 3.80 (p, $J = 6.3$ Hz, 1H), 2.68 (m, 1H), 2.58 (t, $J = 6.6$ Hz, 1H), 1.70 (d, $J = 6.9$ Hz, 1H), 1.67 (d, $J = 6.9$ Hz, 1H); ^{13}C NMR δ 174.0, 131.8, 130.0, 122.8, 121.9, 53.9, 54.0, 32.3, 27.5, 16.9, 11.9; MS (EI) 129.1 (M^+), 129.1, 84.1, 74.1, 67.1, 55.1; HRMS calcd for $C_6H_{11}N_1O_2$ (M^+) 129.0790, found 129.0794.

***n*-Formylpropargylglycine Phenyl Ester (14).** Yield 0.68 g (88%). 1H NMR (300 MHz, $CDCl_3$) δ 8.25 (s, 1H), 7.39 (t, $J = 7.5$ Hz, 2H), 7.26 (t, $J = 7.2$ Hz, 1H), 7.11 (d, $J = 7.8$ Hz, 2H), 6.84 (br s, 1H), 5.08 (dt, $J = 7.8$, 5.0 Hz, 1H), 2.96 (m, 2H), 2.80 (s, 1H); ^{13}C NMR δ 168.7, 160.7, 129.5, 126.4, 121.2, 72.2, 49.4, 38.5, 22.5; MS (EI) 235.2 (M^+), 170.1, 142.1, 114.1, 94.0; HRMS calcd for $C_{13}H_{18}N_1O_3$ (MH^+) 236.1287, found 236.1291.

Synthesis of *n*-Formylated Phenyl Phosphonates, 1p–10p. The phosphonates were prepared by the route similar to that described by Guo et al. The use of aldehydes with different side chains yielded the series. A general procedure for the preparation of the phosphonates is as follows: Triphenyl phosphite (10.0 g, 32 mmol), *n*-pentanal (4.0 g, 48.5 mmol), and benzyl carbamate (4.9 g, 32 mmol) were dissolved in 20 mL of glacial acetic acid. The solution was stirred at 50 °C for 2 h and then stirred at room temperature for an additional 2 h. The solution was then concentrated by rotary evaporation to yield a viscous, yellow liquid. The liquid was dissolved in 120 mL of methanol and left a 4 °C overnight to yield white crystals (9.7 g, 65% yield).

The above condensation product (5 g, 11 mmol) was dissolved in a solution of 30% HBr in acetic acid (5 mL), and stirred for 1.5 h at room temperature. Water (100 mL) and ethyl ether (100 mL) were added to the reaction, and the resulting mixture was stirred at room temperature for 10 min. Sodium hydroxide (10 M) was added until the aqueous phase reached pH 9. The organic phase was then washed twice with water (50 mL). The addition of 4 M HCl (5 mL) resulted in the precipitation of diphenyl α -amino alkyl phosphonate (3.5 g, 89% yield).

The amino hydrochloride salts were formylated as described by Chen et al.¹⁷ Briefly, EDC (2.1 g, 11 mmol) was added to a solution of formic acid (1.0 g, 22 mmol) in dichloromethane (30 mL) at 0 °C and stirred for 15 min. A solution containing the hydrochloride salt (2.0 g, 6 mmol) and *N*-methylmorpholine (1.1 g, 11 mmol) in dichloromethane (30 mL) was added. The mixture was stirred at 0 °C for 8 h and then at 20 °C for 10 h. The mixture was then washed with 1 N HCl (2 \times 20 mL), saturated $NaHCO_3$ (2 \times 20 mL), and saturated NaCl (1 \times 20 mL). After the organic phase was dried with Na_2SO_4 , the solvent was removed by rotary evaporation to yield a yellow oil (1.5 g, 78% yield) which was carried on directly to the next step.

Diphenyl *n*-formyl alkyl phosphonate (1.5 g, 4.3 mmol) was dissolved in a solution containing 4.5 mmol of NaOH, water (10 mL), and dioxane (10 mL), and the resulting solution stirred at room temperature overnight. The reaction mixture was then washed with ethyl

(16) O'Donnell, M. J.; Wojciechowski, K. *Synthesis* **1984**, 313–315.

(17) Chen, F. M. F.; Benoiton, N. L. *Synthesis* **1979**, 709–710.

ether (10 mL), and the aqueous layer was dried by rotary evaporation. The remaining residue was dissolved in 5 mL of water, brought to pH 8.5 with 2 N NaOH, and filtered through a 0.45 mm filter. The solution was chromatographed on a DEAE column by eluting with a linear gradient of 0–0.5 N (Et)₃NH₂CO₃. The collected fractions were concentrated by rotary evaporation and redissolved in water (3 mL). The product was converted to the lithium salt by cation exchange chromatography (Dowex-Li⁺ form). The collected fractions were lyophilized, yielding **5p** (Li⁺ salt) (0.79 g, 63% yield (29% overall)) as a white powder.

Phenyl [1-(1-*N*-Formylamino)alkyl]phosphonates. Methyl (1p**). Yield 0.38 g (25%); ¹H NMR (300 MHz, D₂O) δ 8.10 (s, 1H), 7.39 (t, *J* = 7.8 Hz, 2H), 7.21 (t, *J* = 7.5 Hz, 1H), 7.16 (d, *J* = 7.8 Hz, 2H), 3.62 (d, *J* = 12.6 Hz, 2H); ¹³C NMR δ 166.1 (d, 5.6 Hz), 132.0, 126.7, 123.0, 37.0 (d, *J* = 151.2 Hz), 17.8; LSIMS-MS(–) 214.1 *m/z* (MH[–] – HCl).**

***N*-Cbz-aminomethyl Phosphonic Acid.** ¹H NMR (300 MHz, D₂O) δ 7.32 (m, 5H), 5.08 (s, 2H), 3.45 (d, *J* = 11.4 Hz, 2H); ¹³C NMR δ 137.7, 129.5, 129.1, 128.8, 67.9, 39.3 (d, *J* = 151.5 Hz); MS (EI) 244.0 (M – H)⁺, 228.0, 197.1, 138.0, 108.1, 90.0, 79.1; HRMS calcd for C₉H₁₂N₁O₃P₁ (M⁺) 245.0453, found 245.0459.

Diphenyl *N*-*t*-boc-aminomethyl Phosphonate. ¹H NMR (300 MHz, CHCl₃) δ 7.18 (m, 5H), 7.06 (m, 10H), 4.97 (s, 2H), 3.82 (dd, *J* = 10.5, 6.0 Hz, 2H) ¹³C NMR δ 129.8, 128.6, 128.3, 128.2, 125.5, 120.5, 67.5; MS (EI) 397.1 (M⁺), 304.1, 289.1, 256.1, 233.0, 215.0, 184.1, 170.1, 140.0, 107.0, 91.1, 77.0; HRMS calcd for C₂₁H₂₀N₁O₄P₁ (M⁺) 397.1079, found 397.1065

Ethyl (2p**).** Yield 0.27 g (32%); ¹H NMR (300 MHz, D₂O) δ 8.05 (s, 1H), 7.38 (t, *J* = 7.8 Hz, 2H), 7.20 (t, *J* = 7.2 Hz, 1H), 7.15 (t, *J* = 7.8 Hz, 2H), 4.47 (st, *J* = 7.5 Hz, 1H), 1.55 (dd, *J* = 15.9, 7.2 Hz, 3H); ¹³C NMR δ 165.7 (d, 5.5 Hz), 132.2, 126.7, 123.2, 43.9 (d, *J* = 153.2 Hz), 17.8; LSIMS-MS(–) 228.2 *m/z* (MH[–] – HCl).

Propyl (3p**).** Yield 0.59 g (44%); ¹H NMR (300 MHz, D₂O) δ 8.16 (s, 1H), 7.39 (t, *J* = 7.5 Hz, 2H), 7.20 (t, *J* = 7.2 Hz, 1H), 7.18 (d, *J* = 8.1 Hz, 2H), 4.15 (ddd, *J* = 14.7, 7.8, 7.2 Hz, 1H), 1.96 (m, 1H), 1.64 (m, 1H), 0.96 (t, *J* = 7.2 Hz); ¹³C NMR δ 166.6 (d, 5.3 Hz), 132.3, 126.9, 123.4, 50.4 (d, *J* = 152.0 Hz) 25.5, 13.0 LSIMS-MS(–) 242.0 (MH[–] – HCl).

Butyl (4p**).** Yield 0.24 g (30%); ¹H NMR (300 MHz, D₂O) δ 8.16 (s, 1H), 7.41 (t, *J* = 7.5 Hz, 2H), 7.22 (t, *J* = 7.5 Hz, 1H), 7.15 (d, *J* = 7.5 Hz, 2H), 4.28 (ddd, *J* = 14.7, 8.4, 7.2 Hz, 1H), 1.87 (m, 1H), 1.71 (m, 1H), 1.50 (m, 1H), 1.36 (m, 1H), 0.98 (t, *J* = 7.2 Hz, 3H); ¹³C NMR δ 166.2 (d, 5.0 Hz), 132.2, 126.7, 123.2, 48.2 (d, *J* = 152.3 Hz), 33.8, 21.4, 15.2; LSIMS-MS(–) 256.3 *m/z* (MH[–] – HCl).

Pentyl (5p**).** Yield 0.79 g (29%); ¹H NMR (300 MHz, D₂O) δ 8.02 (s, 1H), 7.37 (t, *J* = 7.8 Hz, 2H), 7.18 (t, *J* = 6.3 Hz, 1H), 7.15 (d, *J* = 7.8 Hz, 2H), 4.22 (ddd, *J* = 12.0, 8.4, 7.2 Hz, 1H), 1.91 (m, 1H), 1.65 (m, 1H), 1.31 (m, 4H), 0.98 (t, *J* = 6.0 Hz, 3H); ¹³C NMR δ 166.2 (d, *J* = 5.1 Hz), 132.1, 126.7, 123.1, 48.4 (d, *J* = 152.2 Hz), 31.3, 30.1 (d, *J* = 12.6 Hz), 23.9, 15.6; LSIMS-MS(–) 270.3 (MH[–] – Li).

Hexyl (6p**).** Yield 0.47 g (44%); ¹H NMR (300 MHz, D₂O) δ 8.14 (s, 1H), 7.40 (t, *J* = 7.8 Hz, 2H), 7.21 (t, *J* = 7.5 Hz, 1H), 7.17 (d, *J* = 7.8 Hz, 2H), 4.35 (dd, *J* = 16.8, 10.5 Hz, 1H), 1.91 (m, 1H), 1.66 (m, 1H), 1.44 (m, 1H), 1.10 (m, 5H), 0.87 (t, *J* = 7.2, 3H); ¹³C NMR δ 164.1 (d, 4.2 Hz), 132.1, 126.6, 123.1, 48.4 (d, *J* = 152.8 Hz), 28.8, 27.5, 23.5, 20.2, 11.7; LSIMS-MS(–) 284.1 *m/z* (MH[–] – HCl).

2-Methylpropyl (7p**).** Yield 0.25 g (27%); ¹H NMR (300 MHz, D₂O) δ 8.17 (s, 1H), 7.39 (t, *J* = 7.5 Hz, 2H), 7.20 (t, *J* = 7.5 Hz, 1H), 7.16 (d, *J* = 8.4 Hz, 2H), 4.19 (dd, *J* = 17.7, 4.0 Hz, 1H), 2.27 (m, 1H), 1.03 (d, *J* = 6.9 Hz, 3H), 0.99 (d, *J* = 6.6 Hz 3H); ¹³C NMR δ 166.7 (d, *J* = 6.1 Hz), 132.4, 126.9, 123.5, 53.7 (d, *J* = 149.5 Hz), 31.2, 19.9; LSIMS-MS(–) 256.1 *m/z* (MH[–] – HCl).

2-Methylbutyl (8p**).** Yield 0.36 g (20%); ¹H NMR (300 MHz, D₂O) δ 8.17, 8.15 (s, 1H), 7.40 (t, *J* = 7.5 Hz, 2H), 7.20 (t, *J* = 7.8 Hz, 1H), 7.17 (d, *J* = 7.5 Hz, 2H), 4.39, 4.02 (dd, *J* = 18.0, 4.8 Hz, 1H), 1.97 (m, 1H), 1.76 (m, 1H), 1.05, 1.01 (d, *J* = 6.9 Hz), 0.91 (t, 7.2 Hz, 3H); ¹³C NMR δ 166.3 (d, 4.9 Hz), 132.1, 126.6, 123.2, 53.4 (d, *J* = 149.1 Hz), 50.1 (d, *J* = 150.2 Hz), 38.0, 37.6, 29.5, 26.8, 18.6, 17.0, 13.5, 13.3; LSIMS-MS(–) 270.0 *m/z* (MH[–] – HCl).

3-Methylbutyl (9p**).** Yield 0.73 g (36%); ¹H NMR (300 MHz, D₂O) δ 8.13 (s, 1H), 7.40 (t, *J* = 7.8 Hz, 2H), 7.26 (d, *J* = 7.5 Hz, 1H), 7.18 (d, *J* = 7.8 Hz, 2H), 4.54 (dd, *J* = 15.6, 10.8 Hz), 1.66 (m, 2H), 0.96 (d, *J* = 5.4 Hz, 3H), 0.90 (d, *J* = 5.4 Hz, 3H); ¹³C NMR δ 166.4 (d, 5.0 Hz), 132.4, 126.9, 123.4, 47.2 (d, *J* = 152.8 Hz), 40.7, 27.0, 25.4, 23.0; LSIMS-MS(–) 270.0 *m/z* (MH[–] – HCl).

3,3-Dimethylbutyl (10p**).** Yield 0.37 g (22%); ¹H NMR (300 MHz, D₂O) δ 8.12 (s, 1H), 7.39 (t, *J* = 7.8 Hz, 2H), 7.20 (t, *J* = 7.5 Hz, 1H), 7.15 (d, *J* = 7.8 Hz, 2H), 4.35 (dd, *J* = 16.8, 10.5 Hz, 1H), 1.85 (dd, *J* = 14.7, 10.8 Hz, 1H), 1.58 (dd, *J* = 13.8, 11.1 Hz, 1H), 0.91 (s, 9H); ¹³C NMR δ 166.0, 132.4, 126.8, 123.4, 46.5 (d, *J* = 152.8 Hz), 45.0, 31.4; LSIMS-MS(–) 242.0 *m/z* (MH[–] – HCl).

Diphenyl Methyl Phosphonate. ¹H NMR δ 7.34 (t, *J* = 7.8 Hz, 4H), 7.20 (m, 6H), 1.80 (d, *J* = 17.7 Hz, 3H) MS (EI) 248.1, 170.1, 155.0, 94.0, 77.0, 65.0; ¹³C NMR δ 150.2 (d *J* = 8.1 Hz), 129.7, 125.1, 120.4, 11.4 (d, *J* = 143.2 Hz); HRMS calcd for C₁₃H₁₃O₃P₁ 248.0602, found 248.0607.

Phenyl Methyl Phosphonate (11p**).** Yield 0.44 g (80%); ¹H NMR (300 MHz, D₂O) δ 7.43 (t, *J* = 7.5 Hz, 2H), 7.22 (t, *J* = 7.8 Hz, 1H), 7.18 (d, *J* = 7.5 Hz, 2H), 1.42 (d, *J* = 16.5 Hz, 3H); ¹³C NMR δ 154.2 (d, *J* = 6.9 Hz), 132.6, 127.1, 123.8, 14.7 (d, *J* = 138 Hz); LSIMS-MS(–) 171.0 (MH[–] – Li).

Antibody Preparation and Purification. 17E8 was isolated from ascites fluid and purified by affinity chromatography (protein A) as described by Guo et al.⁸

Steady-State Kinetics of the Phenyl Esters. Michaelis–Menton parameters for the substrates were determined by continuous measurement at 270 nm (phenol release $\epsilon = 1400 \text{ M}^{-1}\text{cm}^{-1}$) using a Uvikon 930 (Kontron Instrument) UV–vis spectrophotometer. All assays were performed with cuvette holders thermostated at $24.5 \pm 0.5 \text{ }^\circ\text{C}$ with a Lauda RM6 temperature control unit. Cells of 1 cm path length (0.5 mL) were used in each experiment. The buffer used in all kinetic experiments was 50 mM borate–150 mM NaCl, pH 8.7. The antibody concentrations used in the experiments ranged from 0.2 to 1.4 μM . The concentration ranges of the substrates were as follows: (**2**, **3**) 30 mM to 600 μM , (**4**, **5**, **6**, **7**, **11**, **12**, **13**, **14**) 2.0 μM to 30 mM. All substrates were soluble at these substrate concentrations. The reactions were initiated by adding 20 μL of substrate stock in DMSO to a solution of 13–25 μL of IgG (in PBS) and 455–467 μL of pH 8.7 borate buffer. In the background reactions, the IgG was replaced with PBS. All catalyzed assays were performed in triplicate. The background reactions were performed in duplicate. The catalyzed rate was obtained by subtracting the average of the background reaction rate from the rate of the catalyzed reaction. The data (v vs [S]) from the experiments were fit with the KaleidaGraph (Synergy Software) curve-fitting program using the Michaelis–Menton equation.

Inhibition by the Phosphonates. The phosphonate inhibition experiments were performed by obtaining the steady-state kinetic constants, in an analogous manner as described above, in the presence of fixed concentrations of the phosphonates. In these experiments, the borate buffer contained the phosphonates. Hydrolysis of the phosphonates in the buffer was not detected spectrophotometrically. The background rate constants were identical within error to those measured with the phosphonate-containing buffer. The phosphonate concentrations ranged (**1p**, **10p**) from 140 μM to 7 mM, (**2p**, **3p**, **9p**) from 30 to 300 μM (**4p**, **5p**, **6p**), from 1 to 30 μM , and (**7p**, **8p**) from 120 to 600 μM . The phosphonate solutions were either used upon preparation or immediately stored at $-20 \text{ }^\circ\text{C}$. The norleucine substrate, **5**, was used in all of the inhibition experiments. The kinetic data were analyzed with the use of Lineweaver–Burk plots. The inhibition constant was obtained by plotting the slope ($K_m/V_{\text{max}}(1 + [I]/K_i)$) from the Lineweaver–Burk plots against inhibitor concentration and obtaining the intercept on the [I] axis ($-K_i$).¹⁸

Inhibition by Inactive Substrates. These inhibition experiments were performed by obtaining the steady-state kinetic constants, in an analogous manner as described above, in the presence of fixed concentrations of inactive substrates. The norleucine substrate, **5**, was used in all of the inhibition experiments. In these experiments, the DMSO/substrate stock solutions contain a fixed amount of inactive substrate. The approximate inhibition constant was obtained from the equation $K_{\text{Mapp}} = K_{\text{Mo}}(1 + [I]/K_i)$, where K_{Mapp} was the experimental

Table 1. Steady-State Kinetic Analysis of Transition State Binding of the Homologous Series^a

substrate	k_{cat} (s ⁻¹)	K_M (mM)	k_{cat}/K_M (s ⁻¹ ·M ⁻¹)	$\Delta\Delta G_b$ (kcal/mol)
1 -H	no catalysis			
2 -CH ₃	1.0 ± 0.1	3.4 ± 0.4	290 ± 40	+2.2
3 -CH ₂ CH ₃	0.37 ± 0.03	2.1 ± 0.5	180 ± 40	+2.5
4 -CH ₂ CH ₂ CH ₃	1.4 ± 0.1	0.32 ± 0.04	4500 ± 60	+0.6
5 -CH ₂ (CH ₂) ₂ CH ₃	2.1 ± 0.1	0.18 ± 0.03	12000 ± 1400	0.0
6 -CH ₂ (CH ₂) ₃ CH ₃	1.3 ± 0.1	0.88 ± 0.12	1500 ± 20	+1.2
7 -CH ₂ (CH ₂) ₄ CH ₃	no catalysis			

^aAll reactions were performed in 50 mM borate, 150 mM NaCl (pH 8.70) at 24.5 ± 1.0 °C. The kinetic constants were determined from saturation plots of initial rates versus substrate concentration. Substrate concentrations used are listed in the Experimental Section. The errors shown were obtained from calculated fits (KaleidaGraph-Synergy Software) of the data to the Michaelis–Menton equation. The errors in the k_{cat}/K_M values were from the propagation of the fitted k_{cat} and K_M errors.⁸⁰ All of the catalyzed reactions were inhibited to background levels with saturating concentrations of **5p** (> 25 mM). The $\Delta\Delta G_b$ values were calculated from the equation $-RT \ln[(k_{\text{cat}}/K_M)_X/(k_{\text{cat}}/K_M)_5]$ where R is the gas constant and T is the absolute temperature. X corresponds to a substrate to which **5** is being compared. The detection limit that has been estimated for the 17E8 at pH 8.70 is approximately 5–10 M⁻¹ s⁻¹ for k_{cat}/K_M . This estimate is based on the lowest k_{cat} value detected (**3**) and the highest substrate concentration used, 44 mM (**1**). We believe this to represent an upper detection limit as the k_{cat} value for **3** could be obtained easily and reproducibly.

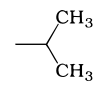
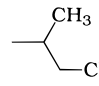
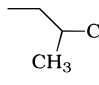
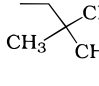
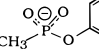
K_M obtained in the presence of inactive substrate and K_{M0} is the K_M obtained in the absence of the inactive substrate. In these experiments it was assumed that the inactive substrates were competitive inhibitors. This assumption is substantiated by the fact there was no change in k_{cat} for norleucine in the presence of these inhibitors.¹⁸

Results

Homologous Series. To investigate the use of binding energy for catalysis between the methylene units of the side chain and the recognition pocket of 17E8, we used a series of phenyl ester substrates and phosphonates that contain aliphatic side chains of varying lengths (Figure 2, **1**–**7**). Table 1 shows the values of k_{cat} , K_M , k_{cat}/K_M , and the relative transition state stabilization energies, $\Delta\Delta G_b$ (relative to **5**) for the series of substrates. Both k_{cat} and K_M values were effected by changing the number of methylene groups in the side chain. The magnitude of these effects varied with respect to each of the steady-state constants. The changes in k_{cat} were the smallest of the three values, spanning a range of about 5-fold (0.4–2.1 s⁻¹). The changes in K_M (0.18–3.4 mM) and k_{cat}/K_M (180–12000 s⁻¹ M⁻¹) are larger—spanning almost 2 orders of magnitude. The values of k_{cat} and k_{cat}/K_M were the largest for **5** and decreased in the order n -propyl **4** ≈ n -pentyl **6** > methyl **2** ≈ ethyl **3**. Removing a methylene group from the side chain decreased $\Delta\Delta G_b$ by as much as 1.9 kcal/mol and as little as 0.3 kcal/mol depending on the position in the side chain. The substrate with no side chain, **1**, showed no detectable activity, as did the substrate with an n -hexyl side chain, **7**. In addition, neither of these substrates competed effectively with hydrolysis of **5**, as there was no change in the k_{cat} or K_M values (data not shown), at high concentrations (44 mM, **1**, and 3 mM, **7**).

Similarly, the K_i values of the corresponding phosphonates (**1p**–**6p**, Figure 3) were affected by the changes in the number of methylene units in the side chain. The K_i values for the phosphonates are shown in Table 2. All of the phosphonates were competitive inhibitors of the catalyzed hydrolysis of substrate **5** (data not shown), suggesting that they bind in the

Table 2. Inhibition Constants of the Phosphonates^a

Inhibitor	K_i (μM)	$\Delta\Delta G_b$ (kcal/mol)
1p -H	1700	+4.8
2p -CH ₃	56	+2.9
3p -CH ₂ CH ₃	30	+2.5
4p -CH ₂ CH ₂ CH ₃	1.2	+0.6
5p -CH ₂ (CH ₂) ₂ CH ₃	0.47	0.0
6p -CH ₂ (CH ₂) ₃ CH ₃	5.3	+1.4
7p 	68	+2.9
8p 	7.2	+1.6
9p 	18	+2.2
10p 	1100	+4.6
11p 	53	+2.8

^aThe constants were determined by plotting the slope values obtained from Lineweaver–Burk plots against inhibitor concentration and obtaining the intercept on the [inhibitor] axis which yields $-K_i$. The slope values are equal to $((K_M(1 + [I]/K_i)/V_{\text{max}}))$. The inhibitor concentrations used to obtain the K_i values are given in the Experimental Section. The $\Delta\Delta G_b$ values were calculated from the equation $-RT \ln[(K_i)_X/(K_i)_{5p}]$. The K_i values were treated as thermodynamic equilibrium binding constants as the nature of inhibition was purely competitive (with respect to **5**) of the 17E8-catalyzed reaction (data not shown).¹⁸

active site of the antibody and that the K_i values represent the thermodynamic binding constants K_d for each phosphonate.¹⁸ The K_i values for this series ranged from 1.7 mM to 470 nM, spanning about 4 orders of magnitude. The order of increasing affinity of the phosphonates to 17E8 mirrors that of the catalytic specificity of the corresponding substrates. The energetic changes, $\Delta\Delta G_b$, reflected by the K_i values for the side chain variation are similar to those for the k_{cat}/K_M values for the corresponding substrates.

Two phosphonates (**1p** and **11p**) were used to probe transition state binding upon complete removal of the side chain. The substrates corresponding to both of the phosphonates are not cleaved by the antibody.¹⁹ The K_i values of **1p** and **11p** are 1.7 mM ($\Delta\Delta G_b = 4.8$ kcal/mol) and 53 μM (2.8 kcal/mol), respectively (Table 2). **1p** is an obvious candidate because, like the rest the homologous series, it serves as a probe for the methylene–pocket interactions without changing other substituents on the molecule. However, the absence of a substituent on the α -carbon introduces the additional complexity of conformational freedom. Thus, the $\Delta\Delta G_b$ for **1p** reflects both the lack of side chain–pocket interactions and the newly introduced rotational entropic requirement for binding the phosphonate.^{20,21} **11p** also serves as a probe for investigating the effects of removing the side chain. In this molecule, extra

(19) The substrate corresponding to **1p** is **1**. The hydrolysis of phenyl acetate, the substrate that corresponds to the phosphonate, **11p**, was not catalyzed by 17E8 (data not shown).

(20) Ramakrishnan, C.; Ramachandran, G. N. *Biophys. J.* **1965**, *5*, 909–933.

(21) Ramachandran, G. N.; Sasisekharan, V. *Adv. Protein Chem.* **1968**, *23*, 283–437.

(18) Segel, I. H. *Enzyme Kinetics*; John Wiley and Sons: New York, 1975; p 957.

Table 3. Steady-State Kinetic Analysis of Transition State Binding of the Branched Series [for accompanying notes see Table 1]

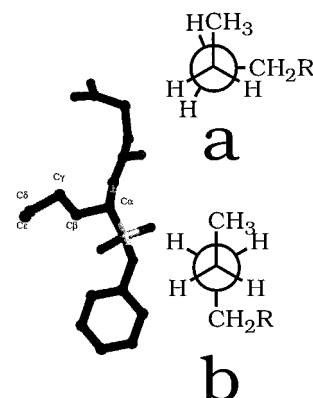
Substrate	k_{cat} (s^{-1})	K_M (mM)	k_{cat}/K_M ($\text{s}^{-1}\cdot\text{M}^{-1}$)	$\Delta\Delta G_b$ (kcal/mol)
8^a 	no catalysis	-	-	-
9 	no catalysis	-	-	-
10 	no catalysis	-	-	-
11 	2.1 ± 0.1	1.6 ± 0.2	1300 ± 200	+1.3

conformational freedom has not been introduced due to the degenerate conformers upon rotation about the $\alpha\text{-C-P}$ bond; however, the interactions between the *n*-formyl group and the protein are lost. Although these molecules were used to investigate the same problem, they have very different binding affinities. The $\Delta\Delta G_b$ values (relative to **5p**) nevertheless indicate that the side chain is very important for phosphonate binding. The anomalous tight binding of **11p** could be a result of restriction of conformation due to the bond deletion, the removal of an unfavorable interaction between 17E8 and the *n*-formyl group, or changes in the solvation properties of the molecule.

Branched Series. We used substrates which were branched at different positions to determine steric and geometric restrictions that govern the interactions between the substrate side chain and the recognition pocket. The kinetic values for these substrates are shown in Table 3. The γ -branched leucine ester (**11**) was a substrate for the antibody, whereas the α - (**8**) and β -branched (**9**, **10**) substrates were not hydrolyzed by the antibody. The k_{cat} value of 2.1 s^{-1} for the leucine substrate (**11**) was similar to that of its linear counterpart **5**, whereas the K_M value is 10-fold higher (1.6 mM), resulting in a decreased k_{cat}/K_M (**11** compared to **5**). The presence of high concentrations of **9** (4 mM) and **10** (2 mM) approximately doubled the K_M value of **5** (relative to the value in their absence—data not shown) with no change in k_{cat} . These results yield the approximate K_i values of 4 mM for **9** and **10**. The presence of a high concentration of **8** did not change the K_M (or k_{cat}) value of **5**.

The K_i values of phosphonates that contain branched side chains (**7p**–**10p**) were also obtained (Table 2). As with the homologous phosphonate series, these were found to be competitive inhibitors of the catalyzed reaction. Phosphonate **9p**, which corresponds to the γ -branched substrate **11**, had a K_i value of $18 \mu\text{M}$ ($\Delta\Delta G_b = 2.2 \text{ kcal/mol}$). The β -branched phosphonate, **7p**, was a respectable binder to the antibody binding site with a K_i value of $68 \mu\text{M}$, whereas the corresponding substrate **9** was not hydrolyzed by 17E8. Its K_i value is similar to that of **2p**, whose corresponding substrate was cleaved by the antibody. We did not use a substrate that corresponded to phosphonate **10p**, but this molecule was of interest because it contained a bulky side chain which would presumably require large structural changes in the recognition pocket for binding. The K_i of 1.1 mM is much larger than those of the homologous series. The energetic changes for binding these phosphonates, **7p** and **10p**, relative to the phosphonate **5p** are 2.4 and 4.0 kcal/mol, respectively.

Conformationally Restricted Substrate Series. The conformationally restricted series was used to investigate the effects of side chain conformation on catalytic activity. The crystal structure of the 17E8-hapten complex suggests the binding of a high-energy hapten side chain rotamer conformation about

**Figure 4.** Bound side chain conformation. (Left) Phosphonate hapten in bound conformation. Coordinates are taken from 17E8-hapten PDB file leap. (Right) Newman projection of the *n*-butyl side chain ($\text{C}\beta\text{-C}\epsilon$). The hapten side chain dihedral angle in (a) bound low-energy eclipsed conformations and (b) low-energy anti conformations.**Table 4.** Steady-State Kinetic Analysis of Transition State Binding of the Conformationally Restricted Series [for accompanying notes see Table 1]^a

Substrate	k_{cat} (s^{-1})	K_M (mM)	k_{cat}/K_M ($\text{s}^{-1}\cdot\text{M}^{-1}$)	$\Delta\Delta G_b$ (kcal/mol)
12 	no catalysis	-	-	-
13^a 	1.4 ± 0.1	0.42 ± 0.07 (0.21 ± 0.04)	3400 ± 700 (6800 ± 1400)	+0.7 (+0.3)
14 	2.8 ± 0.1	1.5 ± 0.1	1900 ± 200	+1.1

^a The prepared substrate was determined to contain a 50:50 mixture of cis and trans isomers (¹H NMR). The values in parentheses are corrected for the actual concentration of the cis isomer. The trans isomer has been shown to be inactive as a substrate.

the dihedral defined by the γ and δ carbons (Figure 4). The substrate containing the side chain with the cis double bond **13** was an active substrate whereas that containing the trans double bond **12** was not hydrolyzed (Table 4).²² There is a small decrease in the k_{cat} value of **13**, relative to that of the linear substrate **5** (2.1 to 1.4 s^{-1}) and essentially no change in K_M (0.18 to 0.21 mM); the k_{cat}/K_M value was decreased only 2-fold (12000 to $6800 \text{ M}^{-1} \text{ s}^{-1}$). The presence of a high concentration of **12** (2.7 mM) approximately tripled the K_M value of **5** relative to its absence (data not shown) with no change in k_{cat} . This result yields an approximate K_i of about 1.6 mM for **12**. The substrate with the alkynyl side chain, **14**, was also processed by the antibody. Its k_{cat} and K_M values are higher than those of the parent substrate **5**. The increased k_{cat} may be solely due to an electronic effect, since the buffer-catalyzed reaction of **14** is increased over that of **5** to the same extent.

Discussion

Nature has evolved many enzymes to use their specificity pockets efficiently. In addition to overall transition state stabilization, these pockets have been experimentally shown to serve several specific roles for catalysis.^{23–27} One role is to assist in the formation of a productive Michaelis complex with the

(22) The substrate **13** was prepared as a 1:1 mixture of the cis and trans isomers whereas **12** was purely trans.

(23) Knowles, J. R. *J. Theor. Biol.* **1965**, *9*, 213–228.

(24) Hedstrom, L.; Farr-Jones, S.; Kettner, C. A.; Rutter, W. J. *Biochemistry* **1994**, *33*, 8764–8769.

(25) Bone, R.; Frank, D.; Kettner, C. A.; Agard, D. A. *Biochemistry* **1989**, *28*, 7600–7609.

(26) Perona, J. J.; Craik, C. S. *Protein Sci.* **1995**, *4*, 337–360.

(27) Thompson, R. C. *Biochemistry* **1974**, *13*, 5495–5501.

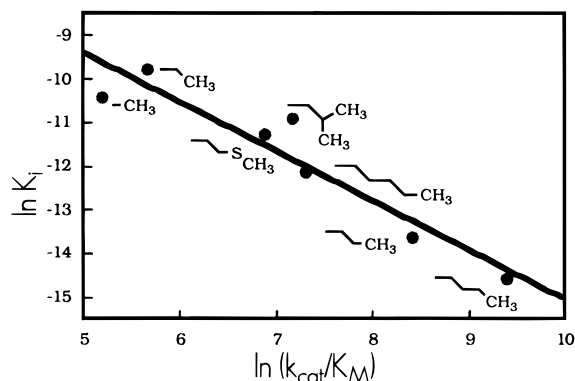


Figure 5. Transition state analogue binding versus catalytic efficiency. $\ln K_i$ vs $\ln k_{\text{cat}}/K_M$ (slope = -1.13 ± 0.17 ; $R = 0.95$). The data were fit with the KaleidaGraph curve-fitting program (data taken from Tables 1, 3, and 4). The inhibition data for the methionine phosphonate will be reported in a future paper.

correct substrates and to hinder the formation of incorrect substrates. A second role is to help precisely position the substrate reactive groups relative to those on other substrates or catalytic groups in the enzyme active site. A third role of specificity pockets is to assist in the preferential stabilization of transition states and high-energy intermediates. Although these are separate roles, nature has coupled them to optimize the efficiency of these interactions in catalysis of specific substrates.^{26,28–31} In this study, we investigate how binding energy in a specificity pocket programmed by hapten design is used in the mechanism of an esterolytic antibody—a protein that has not been optimized by nature to perform catalysis.

Overall Transition State Stabilization. Alternative substrate and transition state analogues provide two different probes to investigate how 17E8's specificity pocket interactions affect the energy of the transition state. There is a good linear correlation between the $\ln(K_i)$ values of the phosphonates and the $\ln(k_{\text{cat}}/K_M)$ values of the corresponding substrates, indicating the presence of similar binding interactions between 17E8 and both the phosphonate inhibitors and the transition states of the catalyzed reactions (Figure 5), suggesting that the inhibitors are good approximations of the transition state.^{32,33} The analogues contain sufficiently different side chains; thus, the correlation implies that the free energy modulation of the transition state complexes is a result of changes in the side chain–pocket interactions and not a result of changes in the catalytic mechanism with the different substrates.

The 17E8 specificity profile resembles that of natural enzymes that contain similar specificity pockets (e.g., chymotrypsin and methionyl-tRNA synthetase).^{34–36} This result is gratifying as this is the first catalytic antibody specificity pocket to be systematically studied. The 2 orders of magnitude range spanned by the substrates' k_{cat}/K_M values is small compared to those of similar substrates with chymotrypsin (4 orders of magnitude) and methionyl-tRNA synthetase (7 orders of magnitude).

(28) Gron, H.; Breddam, K. *Biochemistry* **1992**, *31*, 8967–8971.

(29) Bone, R.; Sheniv, A. B.; Kettner, C. A.; Agard, D. A. *Biochemistry* **1987**, *26*, 7609–7614.

(30) Jencks, W. P. *Proc. Natl. Acad. Sci. U.S.A.* **1981**, *78*, 4046–4050.

(31) Kraut, J. *Annu. Rev. Biochem.* **1977**, *46*, 331–358.

(32) Wolfenden, R. *Annu. Rev. Biophys. Bioeng.* **1976**, *5*, 271–306.

(33) *Transition states of biochemical processes*; Gandour, R. D., Schoenen, R. L., Eds.; Plenum Press: New York, 1978.

(34) Dorovska, V. N.; Varfolomeyev, S. D.; Kazanskaya, N. F.; Klyosov, A. A.; Martinek, K. *FEBS Lett.* **1972**, *23*, 122–124.

(35) Berezin, I. V.; Kazanskaya, N. F.; Klyosov, A. A.; Martinek, K. *FEBS Lett.* **1971**, *15*, 125–128.

(36) Fersht, A. R.; Dingswall, C. *Biochemistry* **1979**, *18*, 1250–1255.

Interestingly, the range of K_i values spanned in the 17E8 system is comparable to ranges seen with thermolysin and α -lytic protease.^{25,37}

The parameters that govern specificity with 17E8 are also similar to those that dictate specificity in enzymatic systems—substrate side chain size, shape, and geometry. The importance of size is best exemplified by the homologous series results which indicate that there is an optimal length for a linear side chain of four carbons. The addition or subtraction of methylene groups to this optimal side chain results in a loss of transition state stabilization. The results with the branched substrates suggest that a linear side chain structure is not required, but only the γ -branching geometry is allowed. This tolerance for only certain side chain branching is also observed with several serine proteases as γ -branching is allowed and β -branching is very detrimental.^{38,39}

A strict conformational requirement to form catalytically productive side chain–pocket interactions is illustrated by the results from the conformationally restricted series in which the side chain with the *cis* double bond (**13**) was a substrate and the side chain with the *trans* double bond (**12**) was not. The torsional angle ($C\beta-C\epsilon$) measured from the refined crystallographic coordinates is approximately 124° (Figure 4). The lowest energy conformation for this torsion angle is 180° .^{40–42} However, in crystallographic models, dihedral angles are difficult to define unambiguously within more than about 20° , especially in cases where the dihedral in question extends beyond the $C\beta-C\gamma$ bond.^{43–45} The kinetic results suggest that the bound conformer of the four-carbon side chain of **5** resembles a high-energy rotamer more closely mimicked by the side chain of **13** and that the conformer mimicked by **12** is one that cannot bind to the antibody.⁴⁶

Another parameter that has been shown to affect specificity in analogous enzyme systems is side chain hydrophobicity. The $\log(K_i)$ and $\log(k_{\text{cat}}/K_M)$ values of the phosphonates and substrates correlate with the hydrophobicity parameter, π (Figure 6, see the caption for the definition of π) which suggests that the hydrophobic effect may provide a large contribution to

(37) Bartlett, P. A.; Marlowe, C. K. *Biochemistry* **1983**, *22*, 4618–4624.

(38) Bigler, T. L.; Lu, W.; Park, S. J.; Tashiro, M.; Wieczorek, M.; Wynn, R.; Michael Laskowski, J. *Protein Sci.* **1993**, *2*, 786–799.

(39) Lu, W.; Apostol, I.; Qasim, M. A.; Warne, N.; Wynn, R.; Zhang, W. L.; Anderson, S.; Chiang, Y. W.; Ogin, E.; Rothberg, I.; Ryan, K.; Laskowski, M. *J. Mol. Biol.* **1997**, *266*, 441–461.

(40) Compton, D. A. C.; Montero, S.; Murphy, W. F. *J. Phys. Chem.* **1980**, *84*, 3587–3591.

(41) Allinger, N. L.; Yuh, Y. H.; Lii, J.-H. *J. Am. Chem. Soc.* **1989**, *111*, 8551–8559.

(42) The energetic difference (ΔH) between the *gauche* and *anti* conformations of *n*-butane is 0.7–1.2 kcal/mol, with the *anti* conformer being preferred. The energetic differences (ΔH) between the two eclipsed forms and the *anti* conformation are 3.5 kcal/mol (H/CH₃) and >4.5 kcal/mol (CH₃/CH₃), respectively (see refs 40 and 41).

(43) Janin, J.; Wodak, S.; Levitt, M.; Maigret, B. *J. Mol. Biol.* **1978**, *125*, 357–386.

(44) Pickett, S. D.; Sternberg, M. J. E. *J. Mol. Biol.* **1993**, *231*, 825–839.

(45) Schrauber, H.; Eisenhaber, F.; Argos, P. *J. Mol. Biol.* **1993**, *230*, 592–612.

(46) However, the energetic cost needed for the antibody to constrain the side chain is not realized with the fixed rotamer mimick (**13**). This conformer is about 3.5 kcal/mol higher in energy than the staggered, low-energy conformer (see refs 40 and 41). Thus, structurally constraining the side chain should allow for this energy to be expressed in greater transition state stabilization. The decrease in activity (Tables 1 and 3) for **13** compared to **5** is most likely a result of the fact that the *cis* isomer does not resemble the bound rotamer precisely due to changes in the hybridization at the δ and γ carbons as well as differences in the dihedral angle between **13** and the actual bound rotamer. The alkene side chain is also less hydrophobic (than **5**), thus raising the desolvation cost for binding. The fact that **14** was also a substrate suggests that the rotameric requirement is only important for the torsion angle defined by carbons C β –C ϵ .

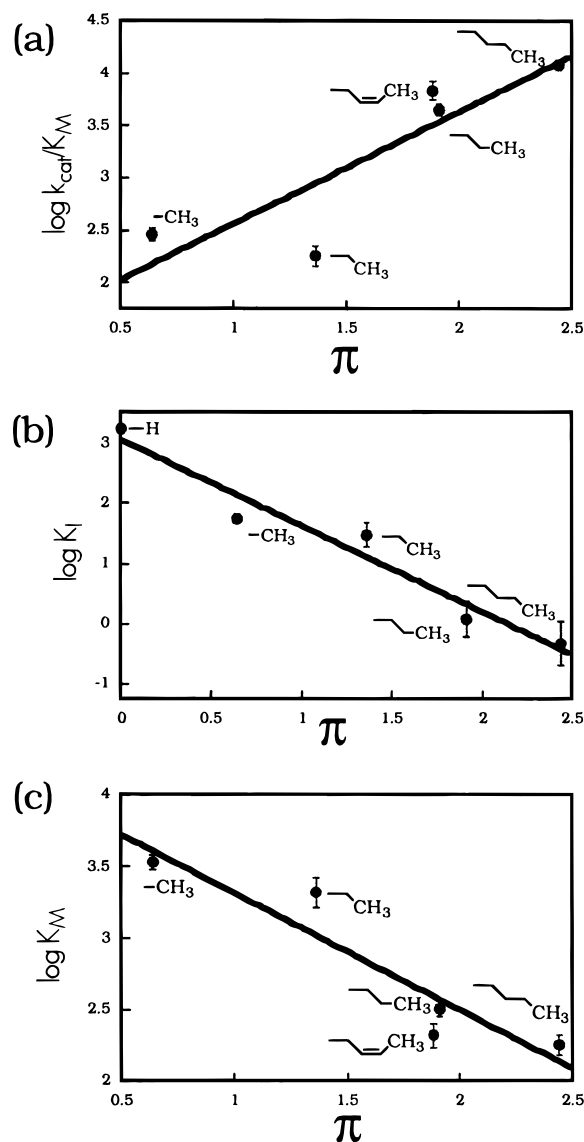


Figure 6. Specificity pocket hydrophobicity. Hydrophobicity (π) of the substrate and phosphonate side chains versus the substrate steady-state kinetic constants and phosphonate inhibition constants where $\pi = \log(P/P_o)$ where P_o is the ratio of the solubility of the parent compound (H-X) in an organic phase to that in the aqueous phase, and P is that of a compound in which the H substituent has been exchanged for R, to give R-X.^{77,78} (a) $\ln k_{\text{cat}}/K_M$ (slope = 1.1 ± 0.4 ; $R = 0.87$). (b) $\ln K_i$ (slope = -1.4 ± 0.2 ; $R = 0.98$). (c) $\ln K_M$ (slope = -0.82 ± 0.20 ; $R = 0.93$).

transition state binding.⁴⁷ This result is supported by the crystal structure of the 17E8·5p complex as the majority of atoms within 5 Å of the side chain carbons are from hydrophobic and aromatic amino acid residues (see Figure 1a).⁹ In studies with chymotrypsin, the $\log(k_{\text{cat}}/K_M)$ values of a series of substrates similar to ours correlated linearly with π as did another serine protease subtilisin which shares a specificity similar to that of chymotrypsin.^{34,35,48} The slopes of the $\log(k_{\text{cat}}/K_M)$ vs hydrophobicity obtained from these enzymatic systems are larger than those obtained from 17E8.⁴⁹

(47) The substrates **6** and **11** (and phosphonates **6p** and **11p**) were not included in the correlations because we believe that these molecules could not be accommodated without changes in pocket structure or binding mode, making the analysis of these compounds ambiguous.

(48) Estell, D. A.; Graycar, T. P.; Miller, J. V.; Powers, D. B.; Burnier, J. P.; Ng, P. G.; Wells, J. A. *Science* **1986**, *233*, 659.

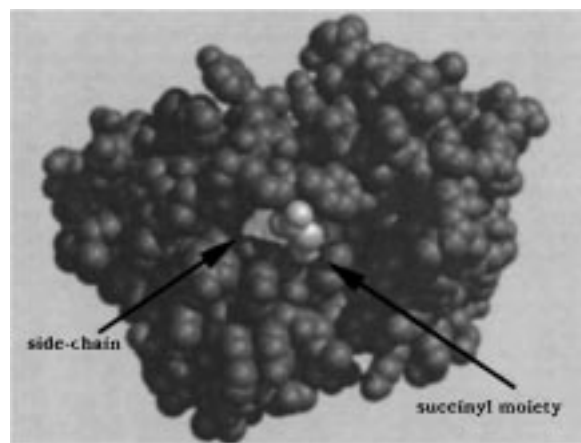


Figure 7. The top view of a space-filling model of the 17E8 (black)·5p (light and dark grey) complex. The model was generated with the MIDAS program.^{75,79}

17E8's active site apparent hydrophobicity results in an average free energy contribution to transition state stabilization per methylene group of about 0.7 kcal/mol. This value is essentially the same as the 0.5 kcal/mol value from experiments in which small molecules were partitioned between the aqueous and organic phases.^{50,51} The negligible difference between the two values does not reflect the expected tighter methylene-pocket interactions in the protein·ligand complexes compared to methylene-organic solvent interactions and the advantage of having a preformed pocket.^{6,52} The $\Delta\Delta G_b$ per methylene group is also significantly smaller than the corresponding values in natural enzymes that contain similar side chain recognition pockets that have evolved to form efficient binding interactions.^{4-6,53} For the enzymatic systems, the $\Delta\Delta G_b$ per methylene group determined from substrate homologous series experiments range from 1.5 to 3.5 kcal/mol. The smaller average value for $\Delta\Delta G_b$ per methylene group indicates that 17E8 does not use binding interactions as efficiently as an evolved enzyme that contains a similar amino acid side chain recognition pocket.

The P1 side chain is completely buried upon the formation of the transition state in serine proteases.^{6,54-56} In contrast, partial solvent accessibility of the hapten side chain is clearly evident in 17E8 (Figures 1b and 7). It has been shown that the partial solvent accessibility of methylene groups in hydrophobic cores results in a reduced contribution to protein stability compared to those that are contained completely in cores.^{57,58} The reduced contribution results from a reduction in the hydrophobic effect and the number of packing interactions. An

(49) Although hydrophobicity may play a major role, there are other factors that are also expected to be major contributors to substrate and transition state binding including statistical entropic factors and enthalpic contributors from the formation of van der Waals packing interactions. Sneddon, F. S.; Tobias, D. J. *Biochemistry* **1992**, *31*, 2842-2846 and Morton, A.; Baase, W. A.; Mathews, B. W. *Biochemistry* **1995**, *34*, 8564-8575.

(50) Rose, G. D.; Wolfenden, R. *Annu. Rev. Biophys. Biomol. Struct.* **1993**, *22*, 381-415.

(51) Pace, C. N. In *Methods in Enzymology*; 1st ed.; Johnson, M. L., Ackers, G. K., Eds.; Academic Press: San Diego, 1995; Vol. 259; p 761.

(52) Richards, F. M. *Annu. Rev. Biophys. Bioeng.* **1977**, *6*, 151-176.

(53) Fersht, A. R.; Shindler, J. S.; Tsui, W.-C. *Biochemistry* **1980**, *19*, 5520-5524.

(54) Perona, J. J.; Hedstrom, L.; Rutter, W. J.; Fletterick, R. J. *Biochemistry* **1995**, *34*, 1489-1499.

(55) Bode, W.; Huber, R. *Eur. J. Biochem.* **1992**, *204*, 433-451.

(56) Stroud, R. M. *Am. Sci.* **1974**, *231*, 74-88.

(57) Jackson, S. E.; Moracci, M.; elMasry, N.; Johnson, C. M.; Fersht, A. R. *Biochemistry* **1993**, *32*, 11259-11269.

(58) Otzen, D. E.; Rhienecker, M.; Fersht, A. R. *Biochemistry* **1995**, *34*, 13051-13058.

extension of this can similarly be drawn to the carbons in the side chain of **5p** and most likely contributes to the apparent unoptimized nature of the 17E8 recognition pocket.

Formation of the Michaelis Complex. 17E8 does use the free energy from the side chain–pocket interactions to stabilize the Michaelis complex. This use of binding energy is especially apparent for the homologous series substrates in which the deletion of each methylene group from **5** (to **2**) results in an increase in K_M . As with the transition state, side chain size, geometry, conformation, and hydrophobicity (Figure 6) affect the free energy of the 17E8 Michaelis complex, lending further support for the participation of the pocket for substrate binding. The K_M increase for the substrates **6**, **11**, and **14** further demonstrates this sensitivity.

The lack of detectable catalysis for **1**, **7–10**, and **12** does not rigorously prove that the substrates cannot form ground-state Michaelis-type complexes with 17E8. To determine the free energies of their Michaelis-type complexes, the approximate K_i values of these compounds were obtained. The free energies for the 17E8 complexes with **9**, **10**, and **12** are 1.4–2 kcal/mol greater than those for the 17E8·**5** complex. The K_i values of **1**, **7**, and **8** could not be obtained because of the solubility limits of the compounds; thus, the free energies corresponding to the K_i values of these compounds must be greater even than those determined. These results lend further support to the side chain–pocket interactions being important for the free energy of the Michaelis complex. Destabilizing interactions are introduced in the case of the long (**7**) and branched (**8–10**) substrates, whereas many of the favorable interactions are removed with the substrate **1**.

Alignment of Catalytic Groups. The side chain–pocket interactions are used to assist in the alignment of the oxyanionic intermediate to the stabilizing cationic center on 17E8. Interestingly, the results from the homologous series indicate that only one methyl group (substrate **2**) is needed for proper alignment of the substrate to the 17E8 catalytic machinery. The k_{cat} values do not increase significantly with the addition of larger side chain groups (from **2** to **6**). The presence of very short (**1**), long (**7**), α - and β -branched (**8–10**), or conformationally incorrect (**12**) side chains results in a loss of detectable catalysis.

One explanation for the lack of catalysis with these substrates may be the inability of the transition states to interact productively with the catalytic center. The high K_i values of the inactive substrates cannot fully account for the lack of detectable catalysis as there are active substrates that have similarly high K_M values. To understand how substrates are discriminated against in the transition state, the binding of transition state analogues (phosphonates) corresponding to the several inactive substrates was investigated. The weak binding of **1p**, and transition state binding, in itself provides a rationale of why the corresponding substrate, **1**, was not detectably hydrolyzed by 17E8. The transition state analogue, **7p**, is a respectable binder (K_d similar to **2p**), although the corresponding substrate, **9**, was not cleaved detectably by 17E8. The ability of this analogue to bind tightly may be due to its potential to bury more hydrophobic surface area (80 Å², **7p**, vs 33 Å², **2p**). This side chain burial must be at the expense of forming efficient interaction with the oxyanion center as evident from the loss of catalysis and the similar binding constant to **2p**. The addition of a methylene unit to the side chain of **7p** results in an increase in binding affinity (**8p**, 101 Å²), supporting the idea that the tight binding of **7p** partly results from the burial of hydrophobic surface area. Nevertheless, the decreases in favorable free energy of the complexes of **7p** and **8p** with 17E8 (+2.9 and +1.6 kcal/

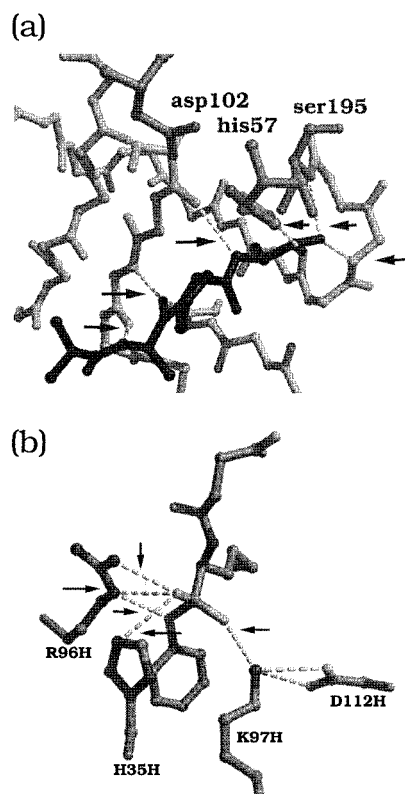


Figure 8. Active site interactions of serine proteases and 17E8. (a) α -Lytic protease complexed with methoxysuccinyl-A-A-P-boroAla.²⁵ Coordinates for the complex were taken from the PDB file lp02. (b) 17E8·**5p** complex. Active site hydrogen bonds are indicated by the arrows. The figures were generated with the MIDAS program.⁷⁵

mol, respectively, relative to **5p**) indicate the stability of these complexes has somehow been compromised. The anomalous tight binding of transition state analogues that correspond to substrates that are not turned over or slowly turned over has also been observed and structurally characterized for α -lytic protease.²⁵ The ability to bury more hydrophobic surface area at the expense of several active site hydrogen bonds is postulated to be one of the reasons for the anomalous binding behavior and loss of catalysis. The prevalence of side chain–pocket interactions in phosphonate, and presumably transition state, binding is also demonstrated with **10p**.

In the serine protease systems, additional subsite binding, active site hydrogen bonds, and the oxyanion hole are used in addition to the interactions in the S1 pocket to obtain the large rate accelerations (Figure 8a).^{29,54,59} Interestingly, this strategy is used by most proteases regardless of the overall tertiary protein structure.⁵⁵ The energy gained from the noncovalent interactions in the specificity pocket is a function of all of these components, some of which are remote from the specificity pocket.^{6,24,60–63} By coupling the S1–P1 interactions to other machinery in the active site, the proteases have created a cooperative network that increases the apparent energy of S1–P1 interactions.³⁰ 17E8 does have a network of interactions that can be used in concert with side chain–pocket interactions. The 17E8 active site contains a center for stabilizing the formation

(59) Hedstrom, L.; Szilagyi, L.; Rutter, W. J. *Science* **1992**, *255*, 1249–1253.

(60) Berti, P. J.; Fearman, C. H.; Storer, A. C. *Biochemistry* **1991**, *30*, 1394–1402.

(61) Ingles, D. W.; Knowles, J. R. *Biochem. J.* **1967**, *104*, 369–377.

(62) Ingles, D. W.; Knowles, J. R. *Biochem. J.* **1968**, *108*, 561–569.

(63) Gron, H.; Meldal, M.; Breddam, K. *Biochemistry* **1992**, *31*, 6011–6018.

of an oxyanion, but it does not use additional subsite interactions to increase the apparent binding energies from the interactions with oxyanion hole (Figure 8b). 17E8 is also missing active site hydrogen bonds that serve as critical kinetic specificity determinants that assist in the more productive use of the side chain pocket binding energy.^{54,62}

Preferential Stabilization of the Transition State. Although overall transition state stabilization increases as methylene groups are added to the side chain of substrates **1–5**, the addition of these units did not significantly increase the k_{cat} values, indicating that the binding energies from the additional methylene–pocket interactions were not used differentially between binding the ground state Michaelis and the transition state complexes. This uniform use of binding energy is thought to be characteristic of an evolutionarily unoptimized catalyst.^{64–66} There are natural enzymes that use much of the binding energy from side chain–pocket interactions for substrate binding specificity and not transition state discrimination.^{11,36,53,67} However, in these systems, kinetic specificity determinants (binding interactions that discriminate at the k_{cat} level only) have also been identified—suggesting that the uniform use of energy from side chain–specificity pocket interactions is permissible as long as there are other sources of differential binding.^{61,62,68–70}

Because they are raised against transition state analogues, and in most cases have been selected for tight binding to these analogues, catalytic antibodies are usually designed to influence only the $E + S^{\ddagger} \leftrightarrow (E \cdot S)^{\ddagger}$ equilibrium—not the equilibria $E + S \leftrightarrow E \cdot S$ and $E \cdot S \leftrightarrow (E \cdot S)^{\ddagger}$. These generation techniques leave no a priori reason for one to expect these proteins to enforce the discriminatory use of remote binding energy between antibody bound species. In fact, the general problem of product inhibition with catalytic antibodies suggests that uniform binding of common moieties on substrates, high-energy intermediates, and products may be prevalent.^{2,71} This is in contrast to enzymes which have evolved to use binding interactions selectively in their mechanisms and not at only one location on the reaction coordinate.^{5,68,72–74} Indeed, a more optimized 17E8 might select against Michaelis complexes that use too much side chain binding energy. In the 17E8 system, the use of the methylene–

pocket interactions to increase k_{cat}/K_M and not to increase k_{cat} makes this clearly a case in which ground-state interactions are inhibitory to increasing the turnover number.³³

Conclusion

In this study, we find that 17E8 does use the binding energy between the *n*-butyl side chain and its recognition pocket to stabilize the bound transition state, indicating that catalytically productive binding interactions that are remote from the catalytic center can be programmed by hapten design. We also find that this pocket has some characteristics similar to those contained in evolved enzymes, including the mechanisms and molecular forces used for specificity. One side chain methyl group is sufficient to ensure high turnover and presumably alignment of the carbonyl group on the ester substrate with the oxyanion hole. Additional methylene groups increase the turnover number almost negligibly but contribute substantially to the formation of the Michaelis complex and catalytic efficiency (k_{cat}/K_M), indicating that 17E8 uses these additional side chain–pocket interactions uniformly in the Michaelis and transition state complexes. This result substantiates the need for selection techniques other than transition state analogue binding in catalytic antibody screening procedures. Optimistically, this suggests that this selection technique may provide a good starting point for a catalyst and that further protein engineering is needed for optimization. The 17E8 side chain–pocket interactions are used less efficiently than those in enzymes as the apparent binding energies gained from the methylene–pocket interactions are significantly smaller in the 17E8 system than those observed in enzymes. Analysis of the 17E8·**5p** complex reveals several possible sources of this reduced apparent binding energy, including incomplete burial of the side chain upon transition state formation and the absence of other binding interactions that could be coupled to the side chain–pocket to preclude wasteful side chain binding. These features provide at least some insight into how 17E8 might be engineered.

Acknowledgment. This study was supported by a grant from the National Institutes of Health (GM 50672). T.S.S. is an Alfred P. Sloan Research Fellow. H.W. is supported by a NSF Predoctoral Fellowship. Mass spectral analyses of synthetic compounds were provided by the UCSF Mass Spectrometry Facility (A. L. Burlingame, Director) supported by the Biomedical Research Technology Program of the National Center for Research Resources, NIH, NCR, BRTP 01614, and NIH NIEHS ES04705. We gratefully acknowledge D. A. Agard, S. M. Miller, and J. Harris for critical review of the manuscript and useful discussions.

JA983017E

(64) Albery, W. J.; Knowles, J. R. *Biochemistry* **1976**, *15*, 5631–5640.
(65) Albery, W. J.; Knowles, J. R. *Angew. Chem., Int. Ed. Engl.* **1977**, *16*, 285–293.

(66) Knowles, J. R.; Albery, W. J. *Acc. Chem. Res.* **1977**, *10*, 105–111.
(67) Mulvey, R. S.; Fersht, A. R. *Biochemistry* **1976**, *15*, 3–249.

(68) Fersht, A. R.; Leatherbarrow, R. J.; Wells, T. C. *Biochemistry* **1987**, *26*, 6030–6038.

(69) Fersht, A. R.; Wells, T. N. C. *Protein Eng.* **1991**, *4*, 229–231.

(70) Wells, T. N. C.; Fersht, A. R. *Biochemistry* **1986**, *25*, 1881–1886.

(71) Lerner, R. A.; Benkovic, S. J.; Schultz, P. G. *Science* **1991**, *252*, 659–667.

(72) Narlikar, G. L.; Herschlag, D. *Biochemistry* **1998**, *37*, 9902–9911.

(73) Avis, J. M.; Fersht, A. R. *Biochemistry* **1993**, *32*, 5321–5326.

(74) Whitty, A.; Fierke, C. A.; Jencks, W. P. *Biochemistry* **1995**, *34*, 11678–11689.

(75) Ferrin, T. E.; Huang, C. C.; Jarvis, L. E.; Langridge, R. *J. Mol. Graphics* **1988**, *6*, 13–27.

(76) Bash, P. A.; Pattabiraman, N.; Huang, C. C.; Ferrin, T. E.; Langridge, R. *Science* **1983**, *222*, 1325–1327.

(77) Fujita, T.; Iwasa, J.; Hansch, C. *J. Am. Chem. Soc.* **1964**, *86*, 5175–5181.

(78) Hansch, C.; Coats, E. J. *Pharm. Sci.* **1970**, *59*, 731–743.

(79) Huang, C. C.; Petersen, E. F.; Klein, T. E.; Ferrin, T. E.; Langridge, R. *J. Mol. Graphics* **1991**, *9*, 230–236.

(80) Bevington, P. R.; Robinson, D. K. *Data Reduction and Error Analysis for the Physical Sciences*, 2nd ed.; McGraw-Hill: New York, 1992; p 328.